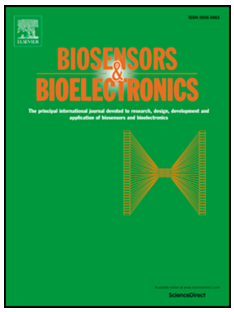

Mobile healthcare system based on the combination of a lateral flow pad and smartphone for rapid detection of uric acid in whole blood

Nan-Si Li, Ying-Tzu Chen, Ying-Pei Hsu, Hao-Han Pang, Chiung-Yin Huang, Yow-Ling Shiue, Kuo-Chen Wei, Hung-Wei Yang

PII: S0956-5663(20)30304-3

DOI: https://doi.org/10.1016/j.bios.2020.112309

Reference: BIOS 112309

To appear in: *Biosensors and Bioelectronics*

Received Date: 8 April 2020

Revised Date: 13 May 2020

Accepted Date: 15 May 2020

Please cite this article as: Li, N.-S., Chen, Y.-T., Hsu, Y.-P., Pang, H.-H., Huang, C.-Y., Shiue, Y.-L., Wei, K.-C., Yang, H.-W., Mobile healthcare system based on the combination of a lateral flow pad and smartphone for rapid detection of uric acid in whole blood, *Biosensors and Bioelectronics* (2020), doi: https://doi.org/10.1016/j.bios.2020.112309.

Nan-Si Li: Methodology, Software, Validation, Formal analysis, Investigation, Writing - Original Draft

Ying-Tzu Chen: Methodology, Investigation, Formal analysis, Resources, Project administration.

Ying-Pei Hsu: Methodology, Investigation

Hao-Han Pang: Methodology, Investigation

Chiung-Yin Huang: Project administration, Resources

Yow-Ling Shiue: Project administration

Kuo-Chen Wei: Conceptualization, Project administration, Resources, Funding acquisition

Hung-Wei Yang: Conceptualization, Methodology, Project administration, Writing - Review & Editing, Supervision, Funding acquisition

Mobile healthcare system based on the combination of a lateral flow pad and smartphone for rapid detection of uric acid in whole blood

Nan-Si Li[#a,b], Ying-Tzu Chen[#b], Ying-Pei Hsu[b,c], Hao-Han Pang[a,b], Chiung-Yin Huang[d], Yow-Ling Shiue[a], Kuo-Chen Wei*[,d], Hung-Wei Yang*[,b]

[a] Institute of Biomedical Sciences, National Sun Yat-sen University, Kaohsiung 80424, Taiwan

[b] Institute of Medical Science and Technology, National Sun Yat-sen University, Kaohsiung 80424, Taiwan

[c] Department of Materials and Optoelectronic Science, National Sun Yat-sen University, Kaohsiung 80424, Taiwan

[d] Department of Neurosurgery, New Taipei Municipal TuCheng Hospital, Chang Gung Memorial Hospital and Chang Gung University, New Taipei City 23652, Taiwan

[#] N. S. Li and Y. T. Chen contributed equally to this work.

Corresponding Author

* E-mail address: kuochenwei@cgmh.org.tw (K.C. Wei)

* E-mail address: howardyang@mail.nsysu.edu.tw (H.W. Yang)

Abstract

Excessive production of uric acid (UA) in blood may lead to gout, hyperuricaemia and kidney disorder; thus, a fast, simple and reliable biosensor is needed to routinely determine the UA concentration in blood without pretreatment. The purpose of this study was to develop a mobile healthcare (mHealth) system using a drop of blood, which comprised a lateral flow pad (LFP), mesoporous Prussian blue nanoparticles (MPBs) as artificial nanozymes and auto-calculation software for on-site determination of UA in blood and data management. A standard curve was found to be linear in the range of 1.5 to 8.5 mg/dL UA, and convenience, cloud computing and personal information management were simultaneously achieved for the proposed mHealth system. Our mHealth system appropriately met the requirements of application in patients' homes, with the potential of real-time monitoring by their primary care physicians (PCPs).

Keywords: Uric acid, colorimetric biosensor, nanozyme, mHealth, smartphone reader

1. Introduction

Uric acid (UA) is produced in the liver by the metabolism of purine from daily intake of nutrients and the endogenous system and is then excreted by the kidneys (Fathallah-Shaykh and Cramer 2014). The normal range of UA levels in whole blood was reported to be 3.5 – 7.5 mg/dL and 2.5 – 6.5 mg/dL for males and females (Ali et al. 2019; Nery 2016), respectively. However, the poor solubility of UA in body fluids causes it to easily precipitate in connective tissue and the urinary system, and long-term hyperuricaemia results in serious complications such as gout, uric acid stones, chronic kidney disease and even fatal cardiovascular diseases (Azmi et al. 2015; Niskanen et al. 2004). To date, various analytical methods for detecting UA such as the phosphotungstic acid method, high-performance liquid chromatography (HPLC), uricase-based photometric or electrochemical methods and commercially available uric acid kits are widely used (Badoei-dalfard et al. 2019; Guo 2016). However, with improving and indulgent lifestyles, hyperuricaemia has become generally common in developed countries, so it is important to monitor the UA concentrations of patients either in blood or urinary excretions in a real-time and on-site way. Many studies have developed different methods to investigate UA in whole blood, serum or urine, such as spectroscopy (Alula et al. 2019; Kumar et al. 2014; Wu et al. 2015) and electrochemistry (da Cruz et al. 2017; Jain et al. 2019; Piermarini et al. 2013; RoyChoudhury et al. 2018). Among these technologies, the costs of instruments and enzymes as well as the requirement of professional technicians are the factors that limit widespread use for mobile healthcare (mHealth) (Zhao et al. 2009). As a result, it has been essential to develop a rapid, easy-to-use, cost-effective, enzyme-free and instrument-free biosensor for on-site UA determination.

Recently, paper-based lateral flow strips have shown many advantages in developing an environmentally friendly, disposable and pattern-customized colorimetric diagnostic platform (Brangel et al. 2018). Consequently, many paper-based studies have shown satisfactory results in detecting UA in

urine, serum or standard samples in buffers (Ali et al. 2019; Islam et al. 2018; Kumar et al. 2015; Wang et al. 2018b). However, because of the inherent white background in paper-based systems of the abovementioned studies, there has been a tendency for the deep colour of serological samples to affect the results. In other words, the test strips could work well for accurate UA detection in standards, urine and serum samples but not directly in whole blood due to their poor signal-to-noise ratio. In addition, these studies have some restrictions for point-of-care (POC) development such as the need for centrifugation pretreatment, expensive optical devices and artificial data analysis. Therefore, the present study is the first to design a custom wax-pattern with three independent zones – sample, detection and background zones – on size-exclusion filter paper to remove the red blood cells and utilize the PEG8000 precipitation method (Pang et al. 2019a; Pang et al. 2019b) to retain large amounts of free haemoglobins and human serum proteins in sample zones to avoid background interferences of serological samples in the working zones and background zones.

Currently, with the first nanozyme research showing that iron oxide nanoparticles possess peroxidase-mimicking catalytic ability similar to that of typical horseradish peroxidase (HRP), researchers have begun to investigate the manufacture of artificial enzymes, so-called nanozymes, which are able to be mass-produced, for example, from metals and their derived materials (Wang et al. 2018a). Among these compounds, ferrous ferrocyanide was the first contemporary synthetic dyestuff, namely Prussian blue (PB), which is a stable nanoparticle when exposed to light. PB has also been reported as a catalyst to accelerate the reduction of hydrogen peroxide (Qiu et al. 2007; Zhang et al. 2010). Therefore, previous studies have developed PB-based electrochemical (Cinti et al. 2018; Jirakunakorn et al. 2020), colorimetric (Farka et al. 2018; Peng et al. 2019; Zhang et al. 2014) and lateral flow immunochromatographic biosensors (Tian et al. 2020) such as for the detection of hydrogen peroxide, UA, glucose, cancer biomarkers, and macromolecules. In addition, compared with natural enzymes, PB

nanozymes have exhibited excellent thermal stability. On the other hand, mesoporous nanomaterials have been widely applied in analytical, biosensing and drug-delivery fields, exhibiting excellent specific surface areas to load biomolecules or nanoparticles (Jafari et al. 2019; Sábio et al. 2019). Among these nanomaterials, mesoporous silica nanoparticles (MSNs) are well-known carriers in the biomedical field and have generated enormous attention because they can be synthesized by an easily controllable process, thereby regulating their pore size, surface area, loading volume and morphology.

In the present study, an mHealth system was developed by integrating a wax-printed lateral flow pad (LFP), mesoporous Prussian blue nanoparticles (MPBs) as nanozymes, a smartphone and customized auto-calculation software for the on-site detection of UA in whole blood. The oxidized 3,3',5,5'-tetramethylbenzidine (TMB) in the detection area would be reduced by UA to etch a pattern in the detection (D) zone, which is then captured and auto-analysed by a smartphone and customized software to obtain the concentration of UA. A linear range from 1.5 to 8.5 mg/dL, with high convenience, selectivity, sensitivity and stability, was obtained. To our knowledge, this is the first study to evaluate UA concentrations on site by an instrument-free, pretreatment-free and enzyme-free LFP with a smartphone for personal hyperuricaemia diagnosis and monitoring.

2. Experimental Methods

2.1. Materials

Phosphate-buffered saline (PBS), ethanol (~99%), polyethylene glycol 8000 (PEG8000, average Mw 7000 ~ 9000), potassium hexacyanoferrate(III) ($K_3Fe(CN)_6$, ~99%), iron(III) chloride ($FeCl_3$), hexadecyltrimethylammonium bromide (CTAB, ~99%), sodium hydroxide (NaOH), tetraethyl orthosilicate (TEOS, ~98%), (3-aminopropyl)triethoxysilane (APTES, ~99%) and hydrogen peroxide (H_2O_2, ~30%) were purchased from Sigma-Aldrich (St. Louis, MO, USA). Grade No. 6 qualitative filter

paper was obtained from Whatman (UK). The printed wax cubes and ColorQube 8570 printer were purchased from Xerox (USA).

2.2. Apparatus

The roughness evaluation was performed by atomic force microscopy (AFM, D3100, Digital Instrument, Italy). The absorbance spectrum and the zeta potential of the materials were detected with a UV/VIS/NIR spectrometer (MODEL V-700, JASCO, Japan) and dynamic light scattering (DLS, SZ-100, HORIBA, Japan). The images and RGB values were captured and calculated by an iPhone 7 plus. The morphology and energy-dispersive X-ray spectroscopy (EDS) characterization of MSNs and MPBs were obtained by transmission electron microscopy (TEM, H-7500, Hitachi) and scanning electron microscopy (SEM, SU8220, Hitachi). The Brunauer-Emmett-Teller (BET) surface area analysis was conducted by an accelerated surface area and porosimetry system (BET, ASAP 2020, Micromeritics, USA). Thermogravimetric analysis was performed by a thermogravimetric analyser (TGA, Q50, TA Instruments, USA).

2.3. Synthesis of MPBs nanozymes

In this study, we incorporated the Prussian blue (PB) with mesoporous silica nanoparticles (MSNs) to enhance the peroxidation activity toward TMB/H_2O_2 and trap the PB inside the detection (D) zone of the LFP for signal concentration. First, 1 g of CTAB was dissolved in 480 mL of DI-H_2O, and 3.5 mL of NaOH (2 M) was added. Then, 5 mL of TEOS and 0.5 mL of APTES were added dropwise into the above mixture under 800 rpm stirring at 70 °C for 2 h in the dark. The synthesized silica nanoparticles (SNs) were purified by centrifugation at 10,000 rpm for 10 min and rinsed with DI-H_2O and methanol three times. The SNs were resuspended in 120 mL of methanol containing 15 mL of 12 M HCl. The

above mixture was stirred at 70 °C for 12 h followed by washing three times with DI-H_2O to obtain MSNs.

Next, 10 mL of 10 mM $FeCl_3$ and 10 mM $K_3Fe(CN)_6$ was freshly prepared and then homogeneously mixed with 10 mg of MSNs at room temperature for 1 h in the dark. Subsequently, after removing free Fe ions in the supernatant by centrifugation and rinsing three times, the MSNs loaded with Fe^{3+} and $Fe(CN_6)^{3-}$ were resuspended in 10 mL of DI-H_2O, followed by the addition of 100 μL of 30 wt% H_2O_2 for 1 h in the dark to obtain MPBs. Finally, the prepared MPBs were washed with DI-H_2O several times to remove excess H_2O_2.

2.4. Fabrication of wax-printed LFPs

First, the LFPs were prepared by printing the designed pattern on filter papers (Qualitative No. 6, Whatman) using a Xerox ColorQube 8570 wax printer (Fuji, Japan), as shown in Fig. 1. Based on the reasons to increase the efficiency of capillary attraction and erythrocyte filtration, the suitable diameters of the blank zone (B zone), sample zone (S zone) and D zone were 6, 8 and 6 mm, respectively. If the diameters of the zones were designed to be less than 6 and 8 mm, the hydrophilic area would be reduced to affect the efficiency of capillary attraction and erythrocyte filtration after the printed LFP was heated at 160 °C for wax melting. Then, we created two nicks with a width of 2 mm on the circle of the D zone to increase the capillary force to allow more solution to migrate to this zone by capillary action. The printed LFPs were then heated to 160 °C for 3 min to help the wax penetrate the cellulose fibres.

Finally, 5 μL of a high ionic strength solution (PEG8000/2 M NaCl) and 3 μL of 1 mg/mL MPBs were dropped onto the S zone and D zone, respectively, and then dried at room temperature for 5 min. The coated LFPs were sealed in a zipper bag to avoid contamination and dust in the air for long-term storage and further UA determination.

2.5. Stability tests

MPBs and HRP were stored in a vacuum drying oven at 25 and 37 °C. After storage for different periods (1–42 days), the catalytic activities of stored MPBs and HRP were investigated by the addition of H_2O_2/TMB and evaluation of the absorption intensity at 450 nm (A_{450nm}) after the addition of HCl. The activities of the stored MPBs and HRP were determined by comparing their A_{450nm} values with their initial A_{450nm} values at day 0. Meanwhile, the MPB-coated LFPs were also stored at 25 °C and exposed to ambient environment for a period of 14 days. Three microlitres of H_2O_2/TMB was dropped on the D zone of stored LFPs at each time point to investigate their storage stabilities by comparing their greyscale values with their initial greyscale values at day 0.

2.6. Software development for auto-calculation of UA detection

The auto-semiquantification operation must be assisted by a custom black paper mask with two bare circles at the relative interest areas of the D zone and B zone. In simple terms, the algorithm of our MATLAB program would remove the deep black area and define two independent circles at the D zone and B zone to calculate the average RGB values of the pixels in these two circles, the details of software development have been shown in Supporting Information. Subsequently, the program auto-transforms the average RGB values to greyscale values using the following equation:

$$\text{Greyscale value} = 0.299\,R + 0.587\,G + 0.114\,B$$

where R, G, and B are the red, green, and blue colour values from the photograph taken by the smartphone, respectively.

In addition, we designed a batch data processing system, meaning that a batch of images was approved to be input into this program and output simultaneously. The results of normal or abnormal samples from subjects were identified and classified by the format of the file names: a/b.Name-preTest/postTest-male/female. The MATLAB software was authorized by the official educational version (MATLAB 2019a). An imaging box with a direct-current LED light and an insertion slot for a paper strip was designed to subsequently provide stable analysis, the details of imaging box design have been shown in Supporting Information.

2.7. UA determination in serological samples using wax-printed LFPs

For UA determination using LFPs, the D zones of wax-printed LFPs were first coated with MPBs, and 3 μL of TMB/H_2O_2 chromogenic substrate was dropped onto the zones to produce the uniform blue colour in 5 min as the primary optical signal source. Then, one drop (approximately 5 μL) of serum or whole blood spiked with UA at the final UA concentration (0, 1.5, 2.5, 3.5, 4.5, 5.5, 6.5, 7.5, and 8.5 mg/dL) was dropped on the S zone, and 25 μL of running buffer (PBS, pH 7.4) was dropped onto the S zone for capillary flow for 10 min to reduce oxidized TMB (blue colour) in the D zone. Finally, the UA tests were stopped by drying the strips for another 5 min at room temperature. To evaluate the feasibility of the proposed LFPs in on-site UA detection compared with the FDA-approved electrochemical analyser (BeneCheck PLUS, BeneCheck, Taiwan) for real blood samples, serological samples obtained in the morning from normal subjects fasting for at least 10 h and from the same subjects after 1 h of eating foods (i.e., meats and seafood) were collected in anticoagulant lithium heparin tubes. The detection procedures were the same as those described above but with no dilution. The images of completed LFPs placed in the imaging box were captured by an iPhone 7 plus, and the greyscale values of the D zone and B zone were auto-calculated to determine the UA concentration by the executable

software. All the serological samples were freshly collected in anticoagulant lithium heparin tubes in the morning and at least 10 h after the most recent meal.

2.8. Establishment of a cloud computing system

For the purpose of the point-of-care system connecting to patients' primary care physicians (PCPs) and medical clinics, we built a cloud drive server by a network-attached storage system. (Synology, DS118j NAS, Taiwan). The captured images of UA tests could be uploaded to the cloud server by users' smartphones with real-time synchronization updates. After the image input, the in-house auto-semiquantification software output the results of UA detection and synchronized immediately. All authorized users were eligible to access the monitoring results by a login mechanism with their own accounts and passwords, a customized app and a browser. To ensure the safety of private information, all the data transmission was under the HyperText Transfer Protocol Secure (HTTPS), the more details have been shown in Supporting Information. All the processes in the simulation were for academic research in human healthcare and were not associated with any financial interests.

3. Results and Discussion

3.1. Characterization of MPB nanozymes

In this research, we proposed an mHealth system comprising a newly designed LFP, MPB nanozymes as a signal probe, a smartphone (iPhone 7 plus), a customized imaging box and automatic monitoring software for on-site UA determination in serum or whole blood. First, the MPBs were prepared as a colour development agent by incorporating PB into the microchannels of MSNs (Fig. 1A). Second, TMB/H_2O_2 was dropped on the D zone with MPB pre-coating of the fabricated LFP to develop a uniform blue colour; then, the sample containing UA was dropped on the S zone for decolouration of

the developed colour in the D zone (Fig. 1B). Finally, the treated LFP was placed in an imaging box for photograph capture and automatic UA determination by the cloud computing mimicking platform, including cloud storage management and data sharing with PCPs.

MSNs are well-known mesoporous nanomaterials that possess numerous advantages including high surface area, tuneable pore size, low production cost and long-term stability. Thus, ultrasensitive human-made nanozymes for TMB oxidation, MPBs, were prepared by incorporating PB within MSNs. The diameter was increased to approximately 81.3 ± 3.5 nm from 54.1 ± 6.9 nm and part of the microchannel was also filled after incorporation of PB with MSNs, as observed by SEM and TEM; based on EDS, a new Fe signal belonging to PB appeared in the PB-impregnated MSNs compared with the original MSNs (Fig. 2A), indicating that PB was successfully incorporated within the MSNs to form MPBs. The results were also confirmed by UV-Vis spectroscopy and BET analysis. From the UV-Vis spectra, two peaks at approximately 400 and 690 nm were observed in the MPBs compared with MSNs, which were attributed to the electron transfer of the typical mixed-valence structure Fe^{2+}-CN-Fe^{3+} in PB (Cui et al. 2015) (Fig. 2B). From BET analysis, the BET surface area of MSNs was 633.91 m^2/g, with a mesoporous adsorption isotherm and 12.20 nm median pore width; however, the surface area was decreased to 471.23 m^2/g with a 0.06 nm median pore width after PB incorporation, indicating that PB was indeed formed and impregnated into the microchannels of the MSNs (Fig. 2C). Nevertheless, the remaining space can still allow a large amount of chromogenic substrates to enter for peroxidation with PB to develop a blue colour. Additionally, the thermogravimetric analysis showed that both MSNs and MPBs had excellent thermal-stable structures without significant weight loss when they were heated to 800 °C (Fig. S1).

3.2. Catalytic stability studies of MPB nanozymes

In this study, the catalytic oxidation of TMB by MPBs was detected by UV-Vis spectroscopy (Fig. 3A). It can be found that the MPBs and TMB/H_2O_2 separately do not exhibit obvious adsorption peaks in the range of 500 to 750 nm (Fig. 3A, a and b). However, a strong adsorption peak at 652 nm for oxidized TMB (TMB_{ox}) appeared in the presence of both MPBs and H_2O_2 (Fig. 3A, c). The intensity at 652 nm was significantly decreased after addition of UA to the TMB_{ox} solution, most likely because UA, a reducing agent, would reduce TMB_{ox} and cause decolorization (Fig. 3A, d). The corresponding photograph of TMB solutions presented in the inset of Fig. 3A shows that the colour of the TMB solution changed to deep blue only in the presence of both MPBs and H_2O_2 and further changed to light blue after UA addition, which is attributed to the characteristic absorption peak of TMB_{ox}. The potential colorimetric biosensing mechanism for UA was as follows (Ali et al. 2019):

$$TMB + H_2O_2 \xrightarrow{MPBs} TMB_{ox} + H_2O$$

$$TMB_{ox} + UA \rightarrow TMB_{red} + allantoinate$$

Subsequently, we studied the peroxidation activity of MPBs compared with that of HRP. The absorbance of TMB was measured at 450 nm ($A_{450\ nm}$), which exhibited a similar intensity (approximately 0.7) after oxidization by HRP and MPBs. Then, the measured $A_{450\ nm}$ values of TMB oxidized by HRP and MPBs at different dilutions were compared (Fig. 3B). The results showed that the A_{450nm} values decreased with increasing dilution ratio in the range from 1- to 128-fold, and the measured values for HRP and MPBs were similar at each dilution, indicating that the MPBs have excellent peroxidation activity towards H_2O_2, similar to that of natural HRP. Additionally, the pH did not influence the peroxidation activity of MPBs towards H_2O_2 from pH 3-11, in contrast with HRP (Fig. 3C). Finally, the long-term stability of HRP and MPBs was evaluated after a period of storage time from

1 to 40 days at 25 and 37 °C; the thermal stability was observed by the signal responses of TMB/H_2O_2 with the HRP and MPBs stored at each time point. As shown in Fig. 3D, HRP quickly lost its entire activity after 8 days of storage at 37 °C and could not maintain its efficiency beyond 42 days of storage at 25 °C. In contrast, the MPBs were introduced to oxidize TMB with almost no decay in response, even when stored at 25 and 37 °C for 42 days. Impressively, the MPBs can maintain their complete catalytic activity, with only 8.6% of the initial activity lost after 42 days of storage at 37 °C. Based on the abovementioned results, the peroxidase-like MPB nanozyme demonstrated high catalytic activity towards TMB/H_2O_2 and excellent thermal and pH stability, thus making it appropriate to replace HRP as the signal probe for colorimetric biosensing.

3.3. Fabrication of LFPs

We patterned chromatography paper with black wax to form an LFP with three zones (B, S, and D zones) and flow microchannels, as shown in Fig. 4A. The S zone was designed for loading serological samples and retaining red blood cells via the size-exclusion function and free haemoglobins via the PEG8000 precipitation method. The D zone was coated with trace amounts of MPB nanozymes for the chromogenic reaction of TMB/H_2O_2, followed by decolorization biosensing by capillary-pumped UA from the S zone, and the B zone was set as the colour baseline for calculation and evaluation of colorimetric changes. After heating the wax-printed cellulose paper at 160 °C for 3 min, the wax melted, permeated into the cellulose paper and vertically spread to the back of the paper to form defined areas of hydrophilic paper separated by hydrophobic lines to form LFPs; these patterns provided spatial control of biological fluids for fluid transport from the S zone to the B and D zones by capillary action. If the heating time was longer than 3 min, the melted wax would also spread to both sides of the pattern, reducing the hydrophilic areas and affecting fluid transport. The SEM images also confirmed the

successful fabrication of LFPs. To verify the successful printing of the hydrophobic patterns on the cellulose paper, an obvious demarcation between the areas with and without wax printing was observed before heating (Fig. 4B, a). However, the demarcation disappeared after the paper was heated at 160 °C for 3 min, most likely because the printed wax melted and permeated into the paper (Fig. 4B, b). From the magnification in Fig. 4B, b, the melted wax was uniformly coated on the surface of all fibres under the pattern to cause a smoother surface than that of fibres without the wax coating. The results indicated that the hydrophobic wax pattern was successfully established for fluid transport. After deposition of MPBs in the D zone, SEM was employed to observe the cellulose fibres in detail. As shown in Fig. 4B, c, the successful deposition of MPB nanozymes on the D zone for further colour development was also confirmed, and many nanostructured spheres were quite uniformly interconnected on the fibre surface of the D zone. The fabrication steps were also monitored by atomic force microscopy. As shown in Fig. 4C, a, the wax-melted paper showed a relatively smooth, flat surface. According to the Z-axis altigraph of the wax-melted paper (the detailed values of the Z-axis and distance are reported in Table S1), the maximum ΔZ value (A_1A_2) was approximately 102.75 nm, similar to the relative maximum of its Z-axis scale. Both the distance and ΔZ values of the protrusions on the surface (B_1B_2 and C_1C_2) did not correspond to the diameter of the MPB nanozymes, representing a pure wax-melted LFP. After MPB deposition, the results showed that many MPB nanozymes attached to the fibres, the ΔZ value of D_1D_2 (99.07 nm) and the distances of E_1E_2 and F_1F_2 (99.92 and 94.37 nm, respectively) were closely matched with the diameter of the MP nanozyme (approximately 81.3 ± 3.5 nm) determined by TEM (Fig. 4C, b). In addition, the average roughness (Ra) in the D zone of the LFP after MPB deposition increased to 48.80 nm from 17.52 nm (pure cellulose paper).

3.4. Optimal parameter settings for UA detection using LFPs

To find the optimal conditions for LFP fabrication, we first tested different volumes of MPBs coated on the D zone of LFPs. More MPBs coated on the D zone would generate an obvious blue colour in the presence of TMB/H_2O_2 but also show a clearly coloured background, affecting the greyscale calculation. The results showed that an obvious blue colour appeared when the volume of MPBs coated on the D zone was more than 3 μL; thus, 3 μL of MPBs was chosen for coating the D zone of LFPs (Fig. S2). Subsequently, the D zone with locally concentrated MPBs was tested for obvious signal responses by reacting with optimally trace amounts of chromogenic substrate. The results showed that the developed colour cannot be evenly distributed throughout the area of the D zone when the volume of TMB/H_2O_2 dropped on the D zone is less than or more than 3 μL (Fig. S3); thus, 3 μL of TMB/H_2O_2 was chosen for colour development. Finally, we coated PEG_{8000}/NaCl on the S zone to retain and filter the erythrocytes and haemachrome, allowing LFPs to be used for UA detection in whole blood without sample pretreatment. Therefore, we tried to drop different volumes of whole blood in the S zone to investigate the capacity of LFPs for erythrocyte separation. The results shown in Fig. S4 demonstrate that the volume of filtered liquid was not sufficient to reach the D zone when the dropped volume of blood on the S zone was less than 30 μL. Conversely, the filtered liquid would flow to the D zone when the volume of blood dropped from zone S was more than 30 μL, but the erythrocytes and haemachrome could not be effectively filtered, and the filtered liquid would also overflow into the D zone, which would greatly influence the detection accuracy. Therefore, in this study, the best sample detection volume for UA detection using LFPs was 30 μL.

3.5. Standard curve for UA detection in whole blood using LFPs

Herein, motivated by the high usage rates of smartphones worldwide, we combined a smartphone and our enzyme-free LFPs to build an mHealth system for UA determination because it is an ideal tool

with its large image storage capacity, effective on-site computing, immediate transmission, user-friendly interface, stable power source and particularly optimal-resolution camera for image capturing (Kanchi et al. 2018; Patel et al. 2016). In addition to using a smartphone camera, we programmed auto-semiquantification software by MATLAB, which is a well-known programming language for algorithm development, signal processing and data analysis, to output the greyscale values of the background zones and working zones with direct batches of image inputs, which indicated that it had potential in cloud-computing applications. On the other hand, a lab-made imaging box device with a direct-current LED light, an insertion slot and a paper mask for a paper strip was designed to supply a stable light source and avoid the noise of the 60 Hz power line frequency when the camera captured an image, and the insertion slot could ensure a fixed position, optical path length (or focal length) and consistent pixels for subsequent analysis (Fig. S5). Most importantly, the paper mask was used to separate other negligible areas from the working zone and background zone for the identification of interest areas and computation by our auto-semiquantification software.

The LFPs were then used to determine the concentration of UA. As the concentration of UA increased in serum or whole blood dropped in the S zone, a more deeply coloured pattern in the D zone was produced (Fig. 5A, left), resulting in an increase in the ratio (I/I_0; I_0: greyscale intensity of pre-test, I: greyscale intensity of post-test), which was recorded by an iPhone 7 plus with an auto-semiquantification algorithm. As a result, the standard curve was found to be linear in the range of 1.5 to 8.5 mg/dL (r^2 = 0.983 for spiked blood samples, Fig. 5A, right). The results demonstrated that the LFPs are very sensitive for UA detection; thus, we can dilute the whole blood 30-fold for tests. To further confirm the accuracy of the LFPs for the determination of UA in whole blood, real whole blood samples were collected from three healthy subjects before and after meals. The obtained results were also compared with those obtained using the BeneCheck PLUS multi-monitoring system, and no significant

difference was found between them (Fig. 5B). The deviation rates of UA determination in whole blood were proved to be appropriate and in the range of 97.36–105.18%, and the relative standard deviations were all lower than 4.8% (Table 1). The results demonstrated that the accuracy and reliability of the LFPs combined with smartphones is sufficient for the determination of UA in real whole blood samples and can be satisfactory for daily monitoring/control of hyperuricaemia.

In addition, we investigated the stability of the LFPs and compared the results with those of electrodes of the BeneCheck PLUS multi-monitoring system. There was no significant decay in the catalytic activity of the LFPs stored at room temperature and even exposed to the normal atmosphere for a period of 14 days. Conversely, the electrodes of the BeneCheck PLUS multi-monitoring system became broken and displayed an error signal when they were exposed to the normal atmosphere for only 10 min (Fig. 5C). The results indicated that the LFPs are stable enough and can be stored in any environment.

3.6. mHealth system simulation in the cloud system

For the purpose of achieving practical application of our mHealth system, we set up a cloud system that included a server to automatically determine UA concentrations, an end-user device such as a smartphone, and Internet browsers operated by patients or PCPs to upload their private personal information and the captured images of detected strips as well as monitor their UA concentrations from an auto-generated report. All the operations are demonstrated in Video S1. We confirmed that the proposed mHealth system is a highly convenient, portable, low-cost and user-friendly system for UA monitoring.

4. Conclusion

In this study, we successfully developed a novel mHealth system comprising an LFP, MPB nanozymes, a smartphone, an imaging box and automatic software for instrument-free and on-site determination of UA in whole blood. UA detection was performed by dropping one drop of blood on a disposable LFP, and the concentration could be easily determined by recording the greyscale values in the D zone using a smartphone. In addition, the LFPs were more stable than the electrodes of the BeneCheck PLUS multi-monitoring system when stored in a normal atmosphere, effectively reducing the detection error. Furthermore, real blood samples from healthy subjects before and after meals have been used to prove the UA detection accuracy for our mHealth system compared with the BeneCheck PLUS multi-monitoring system. To our knowledge, this is the first report on instrument-free paper-based biosensor development with erythrocyte filtration activity to achieve UA determination in complex biosystems by the combination of LFPs with an online auto-calculation system. We envisage that this strategy has great potential as a potent tool for daily UA monitoring and uploading results to the cloud for tracking by PCPs.

Acknowledgments

This work was financially supported by the Ministry of Science and Technology, Chang Gung Memorial Hospital, and National Health Research Institutes, Taiwan (R.O.C.), for the financial assistance provided (MOST106-2628-E-110-001-MY3, MOST106-2628-B-110-001-MY4, CORPG3K0091, and NHRI-EX108-10502NI). We would also like to thank the Chang Gung Memorial Hospital Microscopy Core Laboratory for their assistance with the TEM, SEM, and EDS techniques.

References

Ali, M., Khalid, M.A.U., Shah, I., Kim, S.W., Kim, Y.S., Lim, J.H., Choi, K.H., 2019. New J. Chem. 43, 7636−7645.

Alula, M.T., Lemmens, P., Bo, L., Wulferding, D., Yang, J., Spende, H., 2019. Anal. Chim. Acta 1073, 62−71.

Azmi, N.E., Ramli, N.I., Abdullah, J., Abdul Hamid, M.A., Sidek, H., Abd Rahman, S., Ariffin, N., Yusof,

N.A., 2015. Biosens. Bioelectron. 67, 129−133.

Badoei-dalfard, A., Sohrabi, N., Karami, Z., Sargazi, G., 2019. Biosens. Bioelectron. 141, 111420.

Brangel, P., Sobarzo, A., Parolo, C., Miller, B.S., Howes, P.D., Gelkop, S., Lutwama, J.J., Dye, J.M., McKendry, R.A., Lobel, L., Stevens, M.M., 2018. ACS Nano 12, 63−73.

Cinti, S., Cusenza, R., Moscone, D., Arduini, F., 2018. Talanta 187, 59−64.

Cui, F., Deng, Q., Sun, L., 2015. RSC Adv. 5, 98215−98221.

da Cruz, F.S., Paula, F.d.S., Franco, D.L., dos Santos, W.T.P., Ferreira, L.F., 2017. J. Electroanal. Chem. 806, 172−179.

Farka, Z., Čunderlová, V., Horáčková, V., Pastucha, M., Mikušová, Z., Hlaváček, A., Skládal, P., 2018. Anal. Chem. 90, 2348-2354.

Fathallah-Shaykh, S.A., Cramer, M.T., 2014. Pediatr. Nephrol. 29, 999−1008.

Guo, J., 2016. Anal. Chem. 88, 11986−11989.

Islam, M.N., Ahmed, I., Anik, M.I., Ferdous, M.S., Khan, M.S., 2018. Front. Chem. 6, 496−496.

Jafari, S., Derakhshankhah, H., Alaei, L., Fattahi, A., Varnamkhasti, B.S., Saboury, A.A., 2019. Biomed. Pharmacother. 109, 1100−1111.

Jain, S., Verma, S., Singh, S.P., Sharma, S.N., 2019. Biosens. Bioelectron. 127, 135−141.

Jirakunakorn, R., Khumngern, S., Choosang, J., Thavarungkul, P., Kanatharana, P., Numnuam, A., 2020. Microchem. J. 154, 104624.

Kanchi, S., Sabela, M.I., Mdluli, P.S., Inamuddin, Bisetty, K., 2018. Biosens. Bioelectron. 102, 136−149.

Kumar, A., Hens, A., Arun, R.K., Chatterjee, M., Mahato, K., Layek, K., Chanda, N., 2015. Analyst 140, 1817−1821.

Kumar, V., Misra, N., Paul, J., Dhanawade, B.R., Varshney, L., 2014. Polym. 55, 2652−2660.

Nery, E.W., 2016. Analysis of Samples of Clinical and Alimentary Interest with Paper-based Devices, Springer International Publishing, pp. 25−108.

Niskanen, L.K., Laaksonen, D.E., Nyyssönen, K., Alfthan, G., Lakka, H.M., Lakka, T.A., Salonen, J.T., 2004. JAMA Intern. Med. 164, 1546−1551.

Pang, H.H., Chen, P.Y., Wei, K.C., Huang, C.W., Shiue, Y.L., Huang, C.Y., Yang, H.W., 2019a. Theranostics 9, 1752−1763.

Pang, H.H., Huang, C.Y., Chou, Y.W., Lin, C.J., Zhou, Z.L., Shiue, Y.L., Wei, K.C., Yang, H.W., 2019b. Nanoscale 11, 8102−8109.

Patel, S., Nanda, R., Sahoo, S., Mohapatra, E., 2016. Biochem. Res. Int. 2016.

Peng, C., Hua, M.Y., Li, N.S., Hsu, Y.P., Chen, Y.T., Chuang, C.K., Pang, S.T., Yang, H.W., 2019. Biosens. Bioelectron. 126, 581−589.

Piermarini, S., Migliorelli, D., Volpe, G., Massoud, R., Pierantozzi, A., Cortese, C., Palleschi, G., 2013. Sens. Actuators B Chem. 179, 170−174.

Qiu, J.D., Peng, H.Z., Liang, R.P., Li, J., Xia, X.H., 2007. Langmuir 23, 2133−2137.

RoyChoudhury, S., Umasankar, Y., Jaller, J., Herskovitz, I., Mervis, J., Darwin, E., Hirt, P.A., Borda, L.J., Lev-Tov, H.A., Kirsner, R., 2018. J. Electrochem. Soc. 165, B3168−B3175.

Sábio, R.M., Meneguin, A.B., Ribeiro, T.C., Silva, R.R., Chorilli, M., 2019. Int. J. Pharm. 564, 379−409.

Tian, M., Xie, W., Zhang, T., Liu, Y., Lu, Z., Li, C.M., Liu, Y., 2020. Sens. Actuators B Chem. 309, 127728.

Wang, Q., Wei, H., Zhang, Z., Wang, E., Dong, S., 2018a. Trend. Anal. Chem. 105,218−224

Wang, X., Li, F., Cai, Z., Liu, K., Li, J., Zhang, B., He, J., 2018b. Anal. Bioanal. Chem. 410, 2647−2655.

Wu, D., Lu, H.F., Xie, H., Wu, J., Wang, C.M., Zhang, Q.L., 2015. Sens. Actuators B Chem. 221, 1433−1440.

Zhang, X.Q., Gong, S.W., Zhang, Y., Yang, T., Wang, C.Y., Gu, N., 2010. J. Mater. Chem. 20, 5110−5116.

Zhang, W.M., Ma, D., Du, J.X., 2014. Talanta 120, 362−367

Zhao, Y., Yang, X., Lu, W., Liao, H., Liao, F., 2009. Microchimica Acta 164, 1−6.

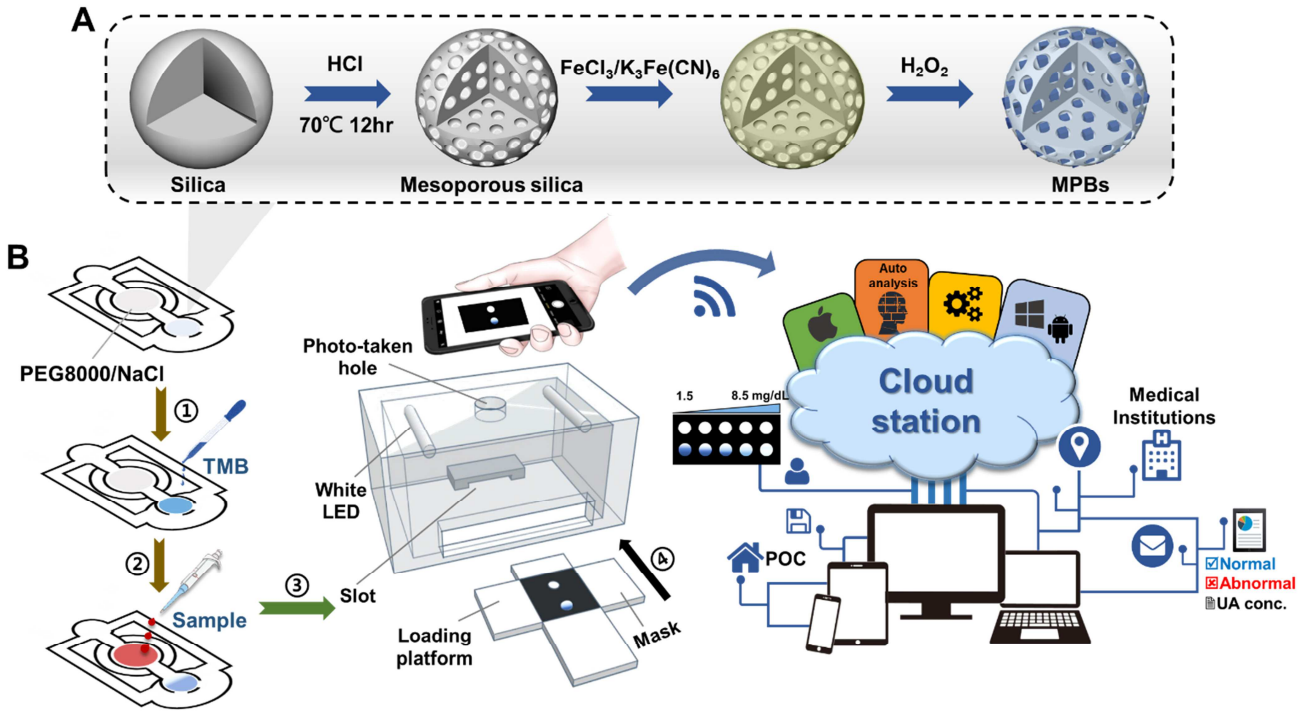

Fig. 1. Illustration of the mHealth system based on the combination of (A) a novel MPB nanozyme, (B) LFPs and a smartphone for rapid detection of UA in whole blood.

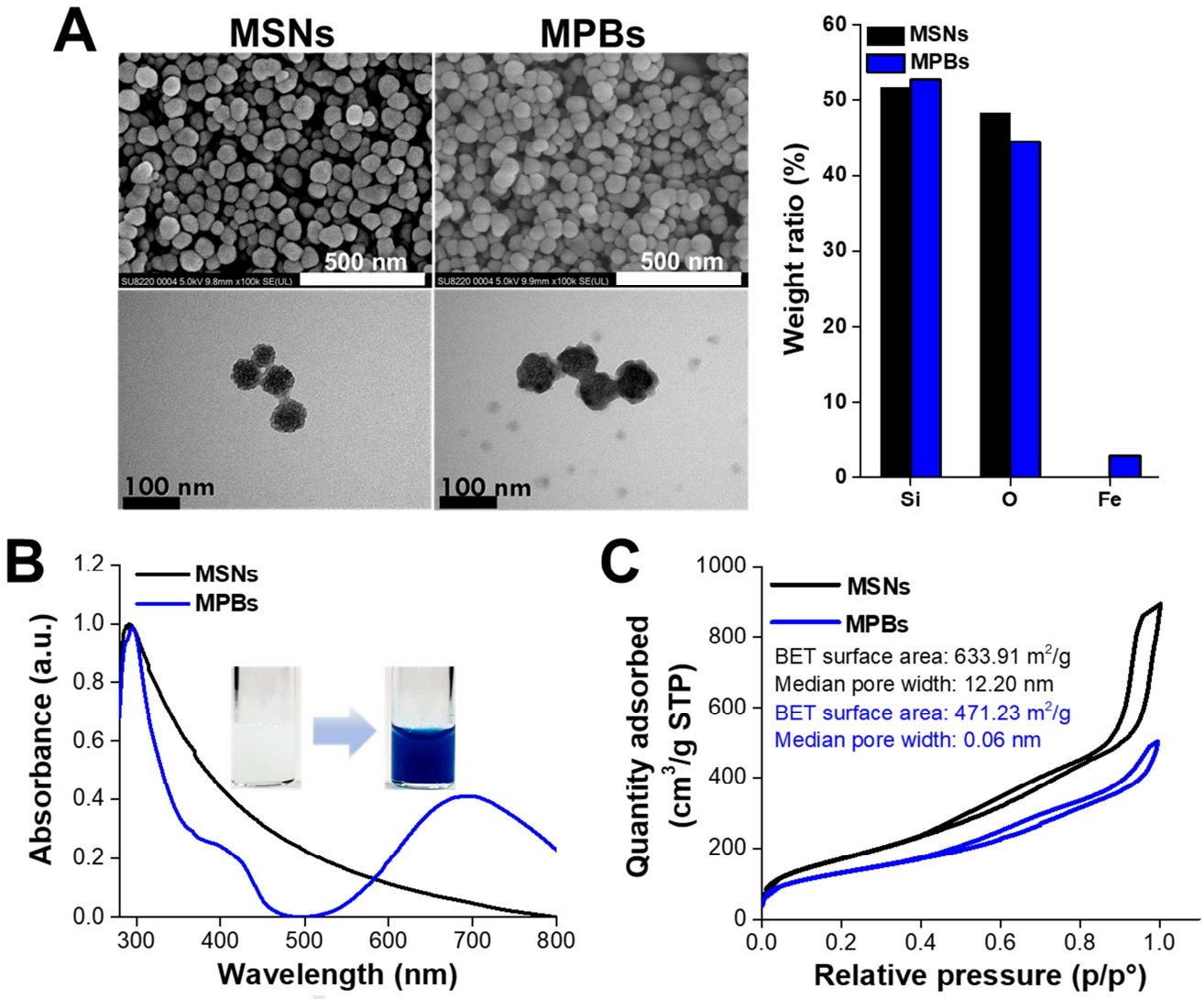

Fig. 2. (A) TEM (top) SEM (bottom) images of prepared MSNs and MPBs; the right inset is their corresponding EDS analysis. (B) UV-vis absorbance spectra of MSNs and MPBs in aqueous solution. (C) The BET adsorption isotherms of MSNs and MPBs with the BET surface area (m^2/g) and median pore width (nm).

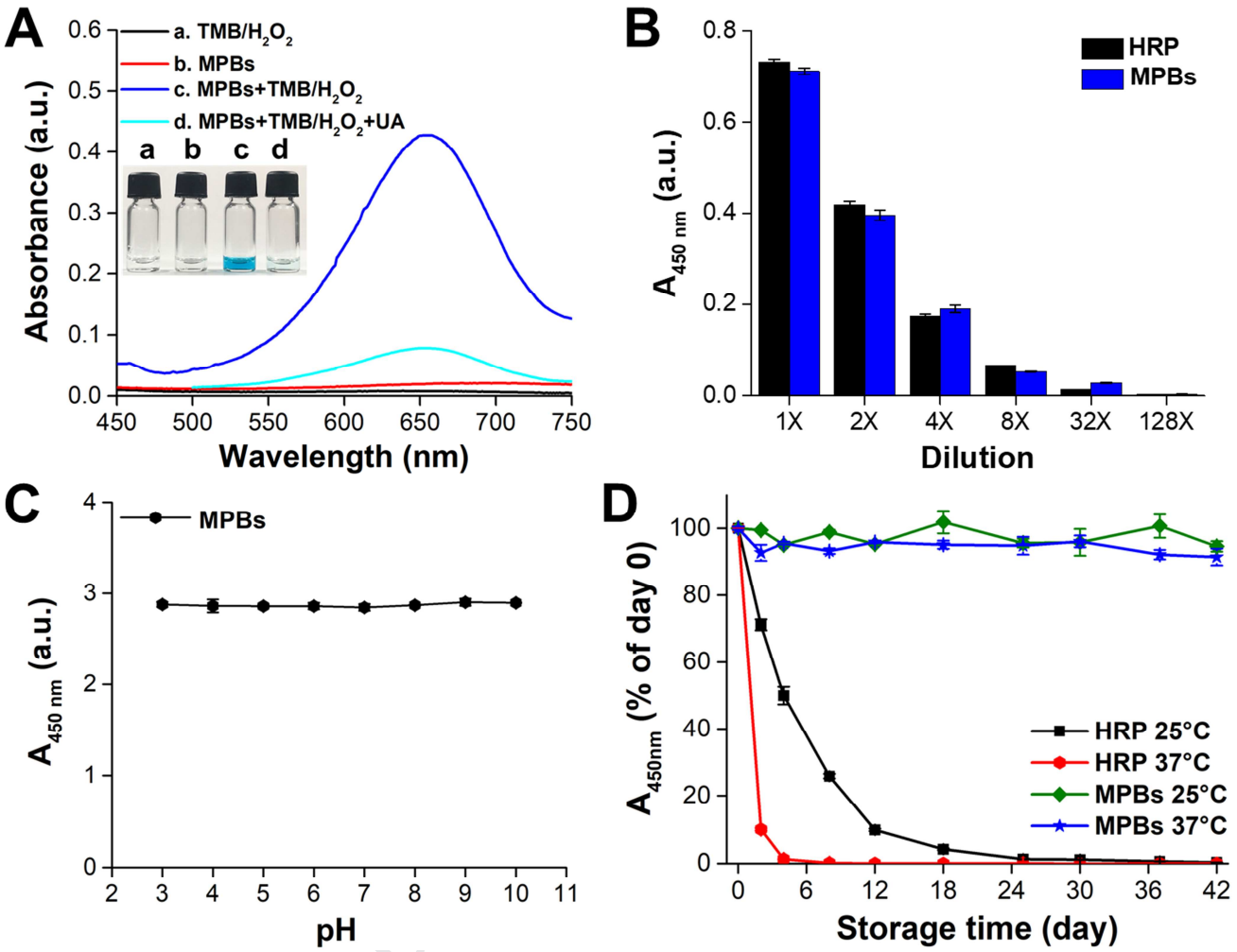

Fig. 3. (A) UV-vis spectrum of different mixtures as follows: (a) TMB/H_2O_2 substrate only, (b) MPB nanozyme only, (c) MPB nanozyme reacted with TMB/H_2O_2 for chromogenic reaction, and (d) MPB nanozyme reacted with TMB/H_2O_2 followed by the addition of UA solution. The inset is the corresponding digital photograph. (B) Comparison of the oxidization with serially diluted HRP and MPBs using TMB/H_2O_2 (n = 3). (C) Stability of prepared MPBs incubated at distinct pH values for 2 h. The stability was evaluated by comparison of the resulting A_{450nm} values for TMB/H_2O_2 oxidation (n=3). (D) Stability of HRP and MPBs stored at 25 °C and 37 °C for a period of 1–42 days. The stability was evaluated by comparison of the A_{450nm} values with the initial value at day 0 for TMB/H_2O_2 oxidation with fresh MPBs (n=3).

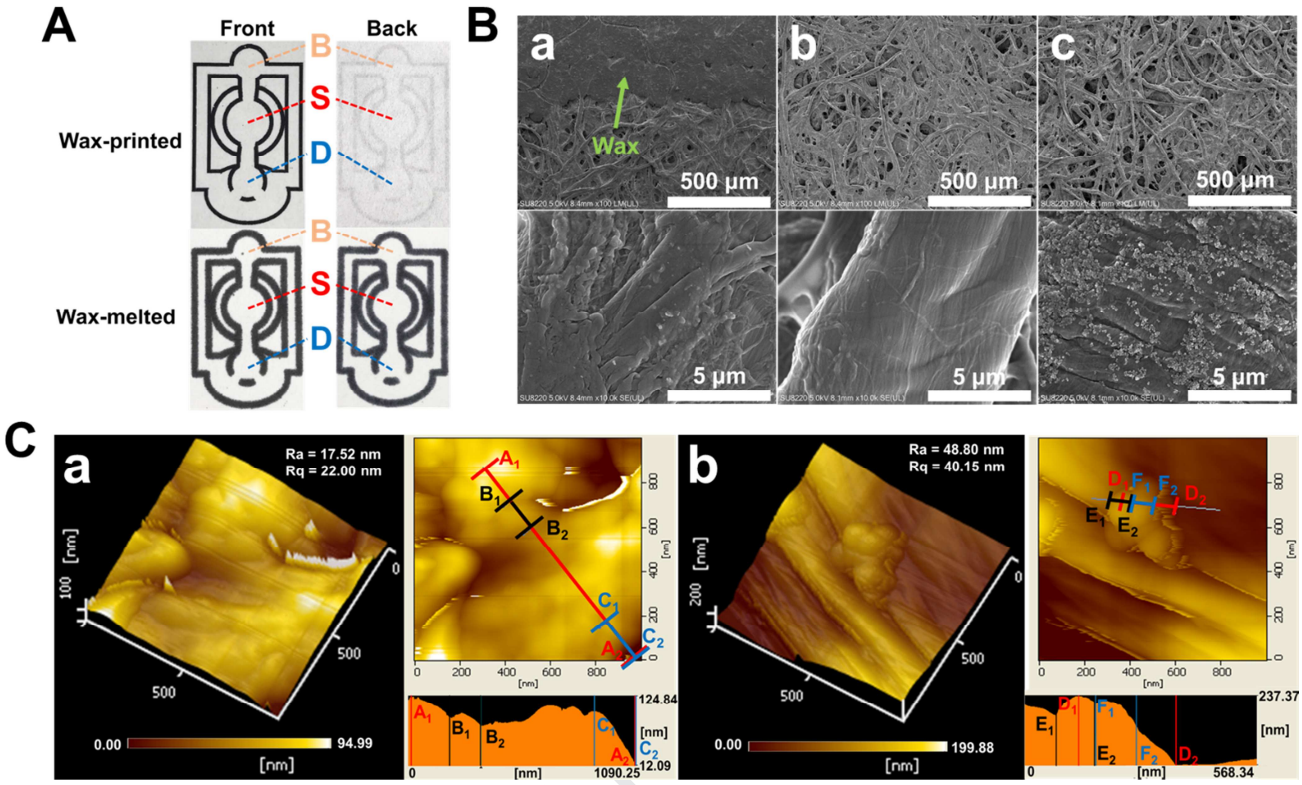

Fig. 4. (A) Photographs of the wax-printed customized patterns of the lateral flow strips before and after heating to be melted. B: The background zone for background evaluation; S: The sample zone for loading samples; and D: The detection zone for colorimetric biosensing. (B) SEM images of (a) the border of wax-printed paper, (b) the border of wax-melted paper and (c) the MPB-coated D zone. The scale bars are 5 and 500 μm. The green arrows show the uniformly printed wax. (C) AFM images of 3D, 2D and Z-axis altigraphs of the working zone of the wax-melted strip (a) before and (b) after MPB nanozyme coating.

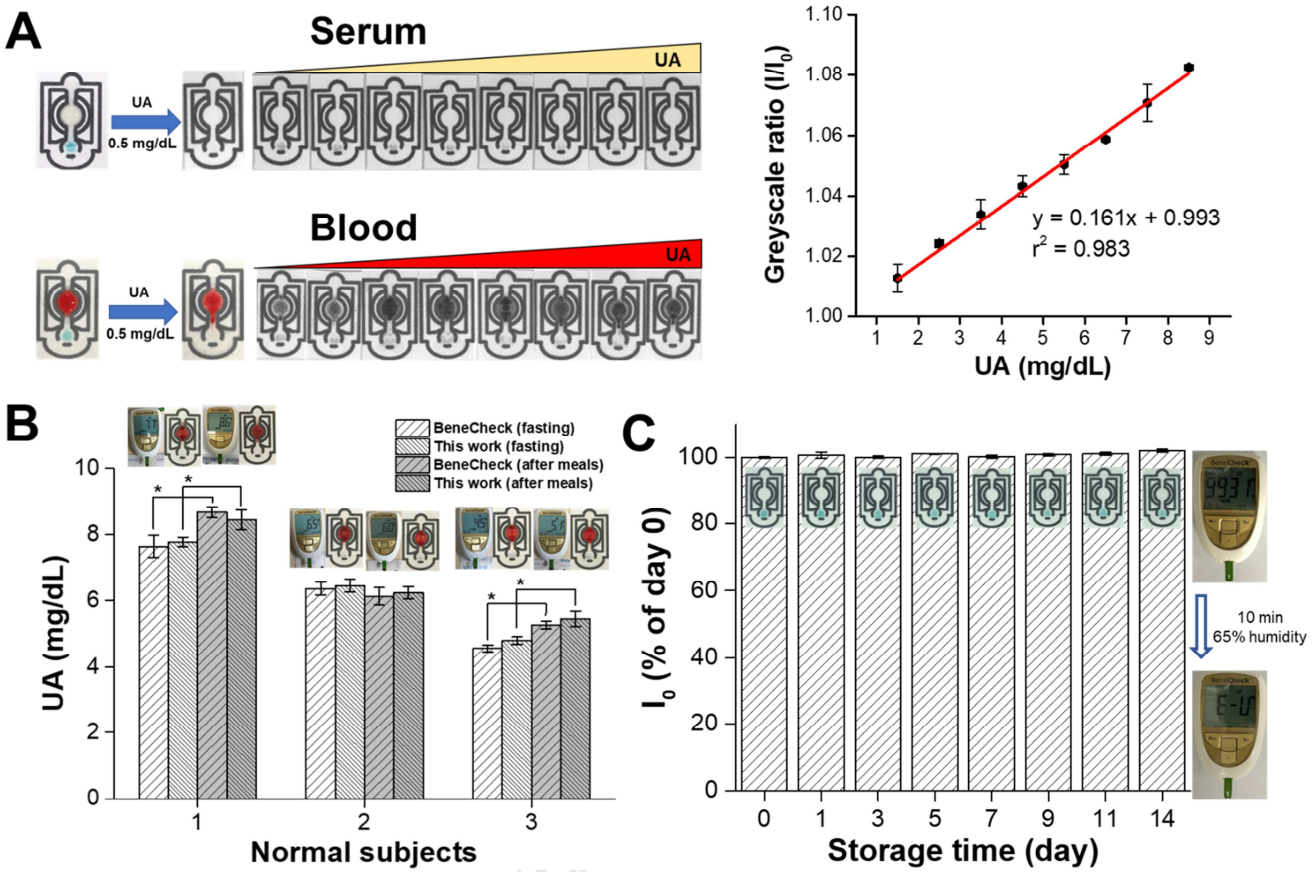

Fig. 5. (A) Photographs of LFPs for UA detection in serum or whole blood and the corresponding linear calibration curve between the greyscale ratio and the concentration of UA in whole blood recorded by an iPhone 7 plus (n = 6). (B) Determination of UA in human whole blood collected from healthy subjects fasting and after meals via the prepared LFPs compared with the FDA-approved BeneCheck system (n = 3). The asterisk indicates a significant difference (Student's t-test, $*p < 0.05$). (C) Stabilities of the as-prepared LFPs exposed to an ambient environment for a period of 14 days and comparison of the results with those of electrodes of the BeneCheck PLUS multi-monitoring system (n = 3). The asterisk indicates a significant difference (Student's t-test, $*p < 0.005$). I_0: greyscale intensity of the pre-test, I: greyscale intensity of the post-test.

Table 1. The deviation rate of the proposed mHealth system (n = 3).

Subjects (Fasting at least 10 h)	Detected (BeneCheck, mg/dL)	Detected (LFPs, mg/dL)	*Deviation (%)	RSD (%)
1	7.63 ± 0.33	7.77 ± 0.14	101.83	1.82
2	6.37 ± 0.19	6.46 ± 0.20	101.43	3.20
3	4.57 ± 0.09	4.8 ± 0.12	105.18	4.80
(After meals)				
1	8.67 ± 0.17	8.44 ± 0.30	97.36	3.47
2	6.13 ± 0.26	6.24 ± 0.18	101.66	2.97
3	5.27 ± 0.12	5.46 ± 0.23	103.75	4.49

* The deviation rate of this work was evaluated compared with BeneCheck.

Highlights

- Preparation of mesoporous Prussian blue nanoparticles (MPBs) as artificial peroxidase-mimicking nanozymes with high oxidative activity and stability.
- A new lateral flow pad (LFP) can filter erythrocytes for on-site uric acid (UA) determination.
- The LFP combined with a smartphone, cloud computing and data storage could achieve mobile healthcare (mHealth) with a range of 1.5-8.5 mg/dL UA.
- This mHealth LFP offers a reliable approach for daily UA monitoring and tracking by primary care physicians (PCPs).

Declaration of interests

☒ The authors declare that they have no known competing financial interests or personal relationships that could have appeared to influence the work reported in this paper.

☐The authors declare the following financial interests/personal relationships which may be considered as potential competing interests: